



drastically different interatomic distances. Five ruthenium, seven tin, and four cerium atoms are within the coordination sphere of both cerium atoms. The striking structural features in both ternary stannides are short cerium-transition metal distances, which are 304-309 pm Ce-Rh in CeRhSn, 233-246 pm Ce1-Ru and 288-291 pm Ce2-Ru in CeRuSn, close to the sums of the covalent radii (290 pm Ce + Rh and 289 pm Ce + Ru),<sup>16</sup> indicating strong Ce-Rh and Ce-Ru bonding. The shortest interatomic distances in both structures occur for Rh-Sn (277-285 pm) and Ru-Sn (265-290 pm), which compare well with the sums of the covalent radii (265 pm Rh + Sn and 264 pm Ru + Sn). Thus, the Ce-T and T-Sn interactions play the dominant role in chemical bonding in CeRhSn and CeRuSn. In the present work, we perform a comparative study of the chemical bonding in these two compounds as based on density functional *ab initio* calculations. In doing so, we take into account previous calculations as well as experimental XPS studies on CeRhSn.<sup>2,17,18,19,20</sup> Our calculations are based on the single-crystal data given in Ref.<sup>2,9</sup>.

### III. THEORETICAL FRAMEWORK

As a matter of fact, the degree of delocalization of the cerium  $4f$  states depends on the applied pressure as well as on the environment in the crystal. In electronic structure calculations this delicate situation is addressed through various approaches treating the  $4f$  states either as atomic like core states or as part of the valence basis set. This duality was experimentally evidenced in a combined analysis of  $\mu$ SR (muon spin relaxation) and neutron experiments on cerium intermetallic systems, which reveals the existence of magnetic excitations due to both conduction electrons at the Fermi level and well localized  $f$ -electrons.<sup>21</sup> Regarding the local environment, the quantum mixing (hybridization) of the  $4f$  states with those of the ligand states can have large effects as well. This involves chemical bonding properties, which depend on the crystal structure as it is illustrated by the compounds under study.

#### A. Computational method

For the electronic structure calculations we used the augmented spherical wave (ASW) method in its scalar-relativistic implementation<sup>13,14,15</sup>. In the ASW method the wave function is expanded in atom-centered augmented spherical waves, which are Hankel functions and numerical solutions of Schrödinger's equation, respectively, outside and inside the so-called augmentation spheres. In order to optimize the basis set, additional augmented spherical waves were placed at carefully selected interstitial sites. The choice of these sites as well as the augmentation radii were automatically determined using the sphere-geometry optimization algorithm.<sup>22</sup> All

valence states, including the Ce  $4f$  orbitals, were treated as band states. In the minimal ASW basis set, we chose the outermost shells to represent the valence states using partial waves up to  $l = 4$  for Ce as well as  $l = 3$  for Ru, Rh and Sn. The completeness of the valence basis set was checked for charge convergence. The self-consistent field calculations are run to a convergence of  $\Delta Q = 10^{-8}$  Ryd<sup>23</sup> and the accuracy of the method is in the range of about 1 meV regarding energy differences.

#### B. Spin-dependent calculations

Due to the intermediate valent and trivalent natures identified for cerium within CeRuSn we carried out spin-degenerate non-magnetic as well as spin-polarized calculations. Assuming a non-magnetic configuration means that the spin degeneracy is enforced for all species. Of course, such a configuration should not be confused with a paramagnet, which could be simulated either by a supercell calculation with random spin orientations or by calling for disordered local moment approaches based on the coherent potential CPA approximation<sup>24</sup> or the LDA+DMFT scheme.<sup>25,26</sup>

Subsequent spin-polarized calculations with different initial spin populations can lead at self-consistency either to finite or zero local moments within an implicit long range ferromagnetic order. They allow to confirm trends established within the mean-field analysis. Antiferromagnetic (AF) calculations can be carried out to test for the AF ground state. This can be done for instance by enforcing an up-spin orientation for half of the crystallographic sites and a down-spin orientation for the other half thus creating two magnetic substructures. Such a procedure is followed here to identify the AF ground state of CeRuSn, which contains four formula units per cell.

#### C. Assessment of chemical bonding properties

To extract more information about the nature of the interactions between the atomic constituents from electronic structure calculations, the crystal orbital overlap population (COOP)<sup>27</sup> or the crystal orbital Hamiltonian population (COHP)<sup>28</sup> may be employed. The latter has been already used to study chemical bonding in CeRhSn.<sup>2</sup> While both the COOP and COHP approaches provide a qualitative description of the bonding, nonbonding, and antibonding interactions between two atoms, the COOP description in some cases exaggerates the magnitude of antibonding states. A slight refinement was recently proposed in form of the so-called covalent bond energy  $E_{cov}$ , which combines the COHP and COOP to calculate quantities independent of the particular choice of the potential zero.<sup>29</sup> In the present work this covalent bond energy was used for the chemical bonding analysis. In the plots, negative, positive and

zero magnitudes of  $E_{cov}$  are indicative of bonding, antibonding, and nonbonding interactions respectively.

#### IV. RESULTS FOR NON MAGNETIC CONFIGURATIONS

##### A. Site-projected density of states

The site-projected DOS (PDOS) for the two ternary stannides CeRhSn and CeRuSn are given in Fig. 2. In all

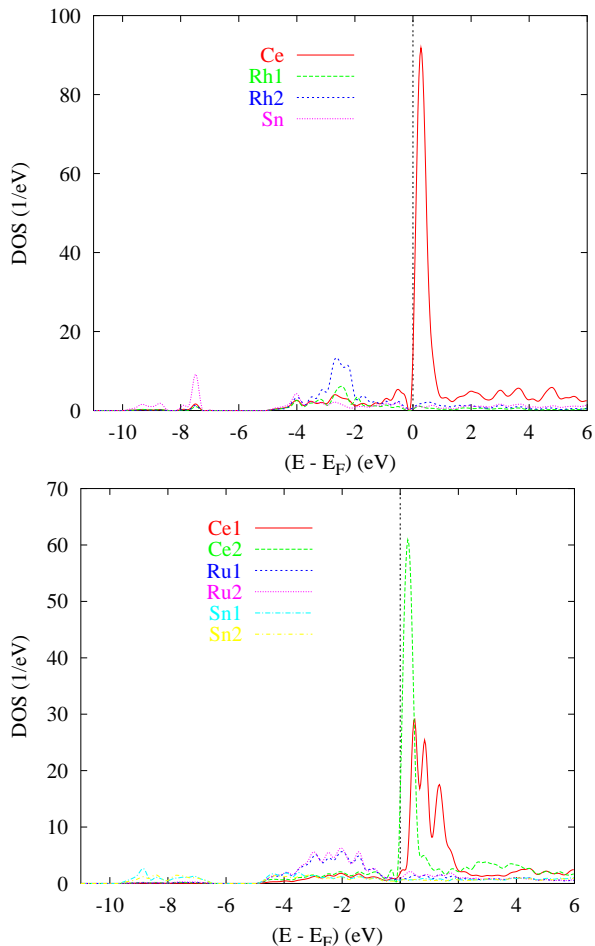


FIG. 2: Non magnetic site projected DOS of CeRhSn (a) and CeRuSn (b)

panels the Fermi level ( $E_F$ ) is taken as zero energy. The cerium DOS are seen to prevail through the large peak around  $E_F$  mainly due to the  $4f$  states. The PDOS of CeRhSn show similarities with the plots obtained from the previous calculations<sup>2,17</sup>, mainly for the itinerant part in the energy range from  $-4$  eV to  $E_F$ , for which Ce XPS spectra were measured.<sup>17</sup> However, major differences occur for CeRuSn, which contains two cerium sites. Broadened Ce1 PDOS are found mainly above the Fermi level with a small contribution at  $E_F$ . In contrast, the Ce2

PDOS are localized at  $E_F$ , which crosses the lower energy part of the Ce  $4f$  states, and behave similarly to the Ce  $4f$  states in CeRhSn. As compared to the latter, the larger splitting of the PDOS, mainly Ce1 as well as Ce2 is due to the lower symmetry of the monoclinic structure of the Ru-based system. There is a non negligible contribution from Ce itinerant states below  $E_F$  which ensure for the chemical bonding through the hybridization with the transition metal (Ru, Rh)  $4d$  and Sn  $5s$  and  $5p$  states. Due to the large filling of their  $d$ -states, the Ru and Rh PDOS are found below  $E_F$ , completely within the valence band (VB). The different PDOS show similar shapes within the VB, mainly in the range from  $-5$  eV up to  $E_F$ , which is indicative of the hybridization of the valence states involving itinerant Ce states below  $E_F$ . We will return to this issue while discussing the chemical bonding in terms of the covalent bond energy  $E_{cov}$  below.

##### B. Analysis of the DOS within Stoner theory

In as far as the Ce  $4f$  states were treated as band states in the framework of our calculations the Stoner theory of band ferromagnetism<sup>30</sup> can be applied to address the spin polarization at the different cerium sites. At zero temperature (ground state) one can express the total energy of the spin system resulting from the exchange and kinetic energies counted from a non-magnetic state as  $E = \frac{1}{2}[\frac{m^2}{n(E_F)}][1 - In(E_F)]$ . Here  $I$  is the Stoner exchange-correlation integral, which is an atomic quantity derived from spin-polarized scalar-relativistic calculations<sup>31</sup>, and  $n(E_F)$  is the DOS at  $E_F$  in the non-magnetic state. From this expression, the product  $In(E_F)$  provides a criterion for the stability of the spin system: A spin-polarized configuration (unequal spin occupation) will be more favourable if  $In(E_F) > 1$ . The system then stabilizes through a gain of exchange energy. From the calculations we have for  $n(E_F)$  for Ce1, Ce2 in CeRuSn and Ce in the rhodium based stannide 11, 98, and 39 states per Ryd, respectively. To analyze these results we use the Stoner integral for Ce as obtained from former scalar-relativistic calculations<sup>33</sup>:  $I(\text{Ce}4f) \sim 0.02$  Ryd. The resulting Stoner products  $In(E_F)$  for Ce1, Ce2 and Ce are, respectively, 0.22, 1.96 and 0.78. The Stoner criterion is obeyed only for Ce2, which should carry a magnetic moment within CeRuSn when spin polarized calculations are carried out. This agrees with its trivalent character versus the intermediate valent character of Ce1. Still, the rather large magnitude of  $In(E_F)$  for Ce in CeRhSn points to a tendency towards a magnetic instability. However, according to the experiment CeRhSn is an intermediate-valence ternary stannide. For this reason, no ordered magnetic moment should develop when spin polarization is allowed for. This is further checked with the spin-polarized calculations outlined in the following section.

### C. Covalent bond energy $E_{cov}$

Chemical bonding properties can be already addressed on the basis of the spin-degenerate calculations. This is due to the fact that the spin-polarized bands, to a large degree, result from the spin-degenerate bands by a rigid energy shift. Negative, positive and zero values of  $E_{cov}$  indicate bonding, antibonding and nonbonding states, respectively.

#### 1. CeRhSn

The covalent bond energies  $E_{cov}$  for the different pairs of orbitals within CeRhSn are shown in Fig. 3. Here, we

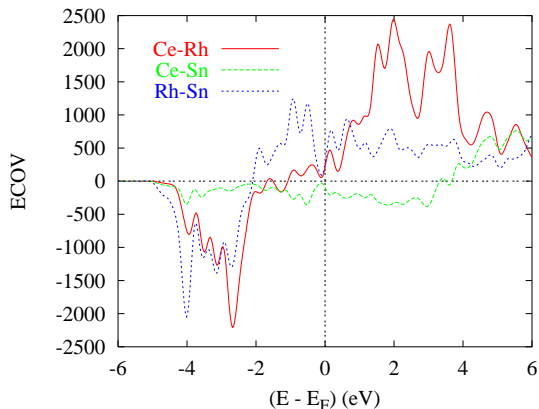


FIG. 3: Chemical bonding: non magnetic  $E_{cov}$  for CeRhSn.

have combined contributions of both Rh sites in order to keep the representation simple. Again, energies are referred to the Fermi level. Note that the  $E_{cov}$  intensities along the ordinate are unitless and should be considered at a qualitative level. From the bottom of the valence band (VB) up to the Fermi level the dominant interactions result from the Ce-Rh and Rh-Sn bonds, which are found strongly bonding up to -2 eV. While the Ce-Rh bond has a rather nonbonding character up to  $E_F$ , it only starts to be antibonding above  $E_F$  within the empty conduction band (CB). One can also notice an antibonding peak above  $E_F$ , which can also be observed for Ce2-Ru2 in CeRuSn (see Fig. 4) as it will be shown below. To the contrary, antibonding Rh-Sn are observed early within the VB, which destabilizes the system. To conclude, the Ce-Rh bond is evidently the stabilizing contribution, followed by the Ce-Sn one, which is of smaller magnitude. It is interesting to note that, although the definition of the covalent bond energy  $E_{cov}$  is somewhat different from that of the COHP, the same bonding trends of CeRhSn are obtained from the calculations of Schmidt *et al.* using the latter.<sup>2</sup>

#### 2. CeRuSn

Due to the superstructure of this system it is useful to study the interactions within two subsystems separately. The result is presented in Fig. 4. There, only one atom

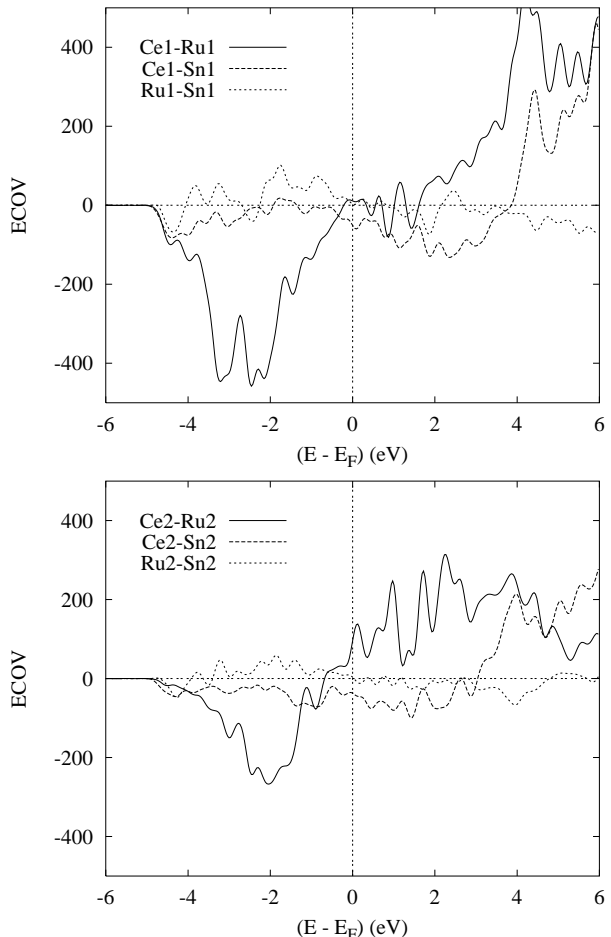


FIG. 4: Chemical bonding: non magnetic  $E_{cov}$  for CeRuSn in two subcells.

of each kind is involved. As a consequence, the absolute  $E_{cov}$  values are smaller than in Fig. 3. The major interactions in the two subsystems occur clearly for Ce-Ru, which is bonding throughout the VB but with twice larger intensity for Ce1 than for Ce2. This follows from the relative distances whereby  $233 < d_{Ce1-Ru} < 246$  pm while  $288 < d_{Ce2-Ru} < 291$  pm. This is concomitant with the different behavior of the two cerium sites as discussed above. The larger Ce2-Ru separation leads to a stronger localization of Ce2 states, which fact is favorable for the onset of an atomic magnetic moment. We also note that the Ce-Rh separation is even larger ( $d_{Ce-Rh} \sim 307$  pm) in CeRhSn. The antibonding peak above the Fermi level just like in the Rh based system is in line with the magnetic instability of Ce2. Finally, albeit with a much smaller magnitude, the Ce-Sn interaction is bonding throughout the VB and should contribute

to the bonding within the system.

## V. RESULTS OF THE SPIN POLARIZED CONFIGURATIONS

Spin-polarized calculations for the magnetic structures were carried out by initially allowing for two different spin occupations, then self-consistently converging the charges and the magnetic moments. We assume firstly a hypothetic ferromagnetic configuration without any constraint on the spins. Then antiferromagnetic computations were carried out for CeRuSn in order to identify the ground state from energy differences.

### A. CeRhSn

Independent of the experimental finding of the intermediate valent character of Ce within CeRhSn, it was suggested from our spin-degenerate calculations as well as from Ref.<sup>17</sup> that the system could be on the verge of a magnetic instability. However, we could not identify a finite magnetic moment on Ce from self-consistent computations at high precision sampling of  $\mathbf{k}$ -space in full agreement with the experiments.

### B. CeRuSn

Contrary to the former system, a stable magnetic solution was identified at high precision BZ sampling. The energy difference favoring the ferromagnetic state is  $\Delta E = 7.14$  meV per formula unit. The spin-only moments were  $M(\text{Ce1}) = 0.005\mu_B$ ,  $M(\text{Ce2}) = 0.44\mu_B$ ,  $M(\text{Ru1}) = -0.015\mu_B$  and  $M(\text{Ru2}) = -0.041\mu_B$ . While the vanishingly small moment of Ce1 resembles the results of CeRhSn, the finite moment on Ce2 is in agreement with the experimental finding as to the trivalent behavior of cerium. The magnetic moments on Ru1 and Ru2 are of induced nature through the hybridization of their states with the respective Ce1 and Ce2 states. These results are illustrated at Fig. 5 showing the site and spin projected density of states of CeRuSn. Low lying Sn 5s states are not shown and the energy window from  $-6$  to  $6$  eV shows the different behavior of the different Ce sites, whereby the exchange splitting is observed only for Ce2. The main bonding characteristics follow the discussion above of the non magnetic DOS.

Spin-orbit coupling effects can be large in Ce based magnetic systems. This is because the localized character of the  $4f$  wave function leads to the formation of orbital moments. We use the orbital field (OR) scheme introduced by Brooks<sup>31</sup> as well as Sandratskii and Kübler<sup>32</sup>, which helped to account for the experimental moments within formerly studied Ce intermetallic systems<sup>33,34</sup>. The trend is that the magnitude of the orbital moment (L) is close to that of the spin-only (SO) moment but with

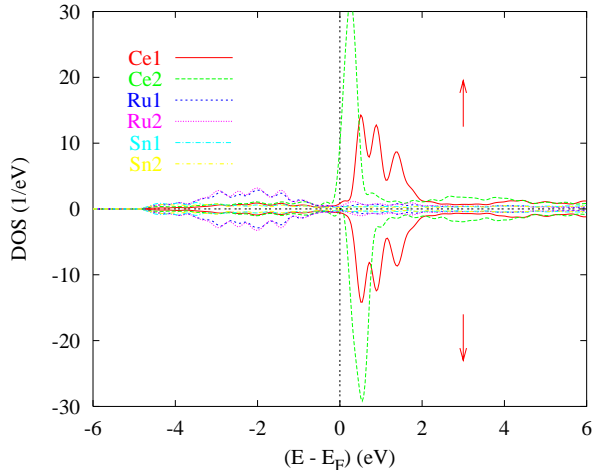


FIG. 5: Site and spin projected DOS of CeRuSn in the ferromagnetic hypothetical state.

opposite signs, in agreement with Hund's 3rd rule. The L moment of cerium stems from a  $4f(\text{Ce2})$  occupation of  $\sim 1.3$  electrons whose orbital moment ( $\sim 2.5\mu_B$ ) comes close to the one of an atomic orbital, namely  $3\mu_B$  as expected from Hund's 2nd rule. This reflects an atomic-like character of the  $4f$  (Ce) subshell. A resulting ordered LS moment of cerium of  $\sim 2\mu_B$  is then obtained; it should be confronted with experimental magnitudes of magnetization from neutron diffraction when the results are made available.

Lastly, in order to check for the ground state, AF calculations were carried out. At self consistency,  $\Delta E = -2.3$  meV in favor of antiferromagnetic ordering was obtained thus pointing to an antiferromagnetic ground state in agreement with the experiment. The moment carried by Ce2 is  $\pm 0.39\mu_B$ , slightly smaller than in the ferromagnetic configuration. This is likely due to the decrease of symmetry when the two magnetic substructures were accounted for within the unit cell.

## VI. CONCLUSION

In this work we have undertaken theoretical investigations of the two ternary equiatomic cerium stannides CeRhSn and CeRuSn as based on accurate X-ray determinations. Calculated densities of states and chemical bonding properties for CeRhSn agree very well with former theoretical results. CeRuSn is strongly influenced by the peculiar feature of a complex interplay of both intermediate valent and trivalent Ce atoms. The exciting properties of this compound were addressed both by spin-degenerate and spin-polarized density functional theory based calculations. Analysis of the electronic structures and of the chemical bonding reveal different types of chemical bonds due to the nature of the Ce site and its environment with Ru, Sn as well as Ce ligands. As a

consequence, a local magnetic moment is expected only for the cerium site with trivalent character. Indeed, spin-polarized calculations lead to a nearly vanishing magnetic moment at the intermediate-valent Ce1 site and a finite moment shows up only at the trivalent Ce2 site. In agreement with experimental data, the Ce2 moments give rise to an antiferromagnetic ground state.

### Acknowledgments

Fruitful discussions with E.-W. Scheidt are gratefully acknowledged. Computational facilities were provided

within the intensive numerical simulation facilities network M3PEC of the University Bordeaux 1 partly financed by the "Conseil Régional d'Aquitaine". This work was supported by the Deutsche Forschungsgemeinschaft through SFB 484 and SCHE /7-1.

- 
- <sup>1</sup> T. Takabatake, Y. Nakazawa, and M. Ishikawa, Jpn. J. Appl. Phys. Suppl. **26**, 547 (1987).
  - <sup>2</sup> T. Schmidt, D. Johrendt, C. P. Sebastian, R. Pöttgen, K. Łątka, and R. Kmiec, Z. Naturforsch. **60b**, 1036 (2005).
  - <sup>3</sup> B. Chevalier, C. P. Sebastian, and R. Pöttgen, Solid State Sci. **8**, 1000 (2006).
  - <sup>4</sup> D. T. Adroja, S. K. Malik, B. D. Padalia, and R. Vijayaraghavan, Solid State Commun. **66**, 1201 (1988).
  - <sup>5</sup> J. F. Riecken, G. Heymann, T. Soltner, R.-D. Hoffmann, H. Huppertz, D. Johrendt, and R. Pöttgen, Z. Naturforsch. **60b**, 821 (2005).
  - <sup>6</sup> S. Baran, J. Leciejewicz, N. Stüsser, A. Szytuła, A. Zygmunt, and Y. Ding, J. Magn. Magn. Mater. **170**, 143 (1997).
  - <sup>7</sup> M. Lenkewitz, S. Corsépius, and G. R. Stewart, J. Alloys Comp. **241**, 121 (1996).
  - <sup>8</sup> 216, 45, and 51 entries occur for the formulae CeNiSn, CePdSn, and CePtSn in the SciFinder Scholar, version 2007 (<http://www.cas.org/SCIFINDER/SCHOLAR/>)
  - <sup>9</sup> J. F. Riecken, W. Hermes, B. Chevalier, R.-D. Hoffmann, F. M. Schappacher, and R. Pöttgen, Z. Anorg. Allg. Chem. **633**, 1094 (2007).
  - <sup>10</sup> R.-D. Hoffmann, B. Chevalier, J. F. Riecken, U. Ch. Rodewald, F. M. Schappacher, and R. Pöttgen, unpublished results.
  - <sup>11</sup> P. Hohenberg and W. Kohn, Phys. Rev. B, **136**, 864 (1964).
  - <sup>12</sup> W. Kohn and L. J. Sham, Phys. Rev. A, **140**, 1133 (1965).
  - <sup>13</sup> A. R. Williams, J. Kübler and C. D. Gelatt, Phys. Rev. B **19**, 6094 (1979).
  - <sup>14</sup> V. Eyert, Int. J. Quantum Chem. **77**, 1007 (2000).
  - <sup>15</sup> V. Eyert, *The Augmented Spherical Wave Method – A Comprehensive Treatment*, Lect. Notes Phys. **719** (Springer, Berlin Heidelberg 2007).
  - <sup>16</sup> J. Emsley, *The Elements* (Oxford University Press, Oxford, 1999).
  - <sup>17</sup> A. Slebarski, M. Radlowska, T. Zawada, M. B. Maple, A. Jezierski, and A. Zygmunt, Phys. Rev. B **66**, 104434 (2002).
  - <sup>18</sup> A. Slebarski, T. Zawada, J. Spalek, and A. Jezierski, Phys. Rev. B **70**, 235112 (2004).
  - <sup>19</sup> K. Shimada, H. Namatame, M. Taniguchi, M. Higashiguchi, S.-I. Fujimori, Y. Saitoh, A. Fujimori, M. S. Kim, D. Hirata, and T. Takabatake, Physica B **791**, 378 (2006).
  - <sup>20</sup> G. R. Stewart, Rev. Mod. Phys. **73**, 797 (2001).
  - <sup>21</sup> A. Yaouanc, P. Dalmas de Rotier, P. C. M. Gubbens, C. T. Kaiser, P. Bonville, J. A. Hodges, A. Amato, A. Schenck, P. Lejay, A. A. Menovsky and M. Mihalik. Physica B **259-261**, 126 (1999).
  - <sup>22</sup> V. Eyert and K.-H. Höck, Phys. Rev. B **57**, 12727 (1998).
  - <sup>23</sup> V. Eyert, J. Comput. Phys. **124**, 271 (1996).
  - <sup>24</sup> A.M.N. Niklasson, J.M. Wills, M.I. Katsnelson, I.A. Abrikosov, O. Eriksson, and B. Johansson, Phys. Rev. B **67**, 235105 (2003).
  - <sup>25</sup> K. Held, V. I. Anisimov, V. Eyert, G. Keller, A. K. McMahan, I. A. Nekrasov, and D. Vollhardt, Adv. Solid State Phys. **43**, 267 (2003).
  - <sup>26</sup> K. Held, I. A. Nekrasov, G. Keller, V. Eyert, N. Blümer, A. K. McMahan, R. T. Scalettar, T. Pruschke, V. I. Anisimov, and D. Vollhardt, phys. stat. sol. (b) **243**, 2599 (2006).
  - <sup>27</sup> R. Hoffmann, Angew. Chem. Int. Ed. Engl. **26**, 846 (1987).
  - <sup>28</sup> R. Dronskowski and P. E. Blöchl, J. Phys. Chem. **97**, 8617 (1993).
  - <sup>29</sup> G. Bester and M. Fähnle, J. Phys: Condens. Matter **13**, 11541 (2001).
  - <sup>30</sup> J. Kübler and V. Eyert, *Electronic structure calculations, in: Electronic and Magnetic Properties of Metals and Ceramics*, edited by K. H. J. Buschow (VCH Verlagsgesellschaft, Weinheim, 1992), pp. 1-145; Volume 3A of *Materials Science and Technology*, edited by R. W. Cahn, P. Haasen, and E. J. Kramer (VCH Verlagsgesellschaft, Weinheim, 1991-1996).
  - <sup>31</sup> M. S. S. Brooks and B. Johansson, in: *Handbook of Magnetic Materials*, ed. K. H. J. Buschow, Vol. **7** (1993).
  - <sup>32</sup> L.M. Sandratskii and J.Kübler, Phys. Rev. Lett. **75**, 946 (1995).
  - <sup>33</sup> S. F. Matar and A. Mavromaras, J. Solid State Chem. **149**, 449 (2000).
  - <sup>34</sup> S. F. Matar, Phys. Rev. B **75**, 104422 (2007).